JOURNAL OF MATERIALS SCIENCE 30 (1995) 3351–3357

The morphology, chain structure and fracture behaviour of high-density polyethylene

Part II *Static fatigue fracture testing*

B. J. EGAN, O. DELATYCKI
Department of Mechanical and Manufacturing Engineering, University of Melbourne, Parkville, Victoria 3052, *Australia*

High-density polyethylene (HDPE) is being used more and more in critical long-term applications. For this reason it is important to have a strong understanding of those parameters which control the fracture behaviour of HDPE. In Part I of this work, fracture results were presented for eleven HDPE samples tested using a tensile testing machine. Such short-term tests do not accurately reflect the in-service loads on HDPE components, which tend to be low and static. It is, therefore, important to perform fracture tests under long-term static loads. The results of such testing are presented in this paper. The resistance to static fatigue was found to be most strongly dependent on molecular weight. Short branch concentration and short branch length were also found to exert an influence on the resistance to static fatigue. This result is similar to the findings presented in Part I of this work. However, there is some evidence that molecular weight influences fracture behaviour to a greater extent in the long-term tests. Notwithstanding, the similarity between the short-term and long-term results is important. It means that an early indication of the long-term performance of HDPE resins can be obtained from rapid comparative tests conducted using a tensile testing machine.

1. Introduction

The work to be presented here forms part of a detailed research programme aimed at a better understanding of how morphology and chain structure control the fracture behaviour of high-density polyethylene (HDPE). This knowledge is becoming increasingly important due to the growing use of HDPE in critical long-term applications. An example of this would be pipes used in water, sewage and gas distribution systems. To optimize the lifetime of such pipes it is important to know how changing elements of the chain structure, such as short branch content and length, will effect the fracture behaviour.

In Part I of this work [1] results were presented for tests conducted at a constant rate of deflection using a tensile testing machine. Research is often conducted in this mode of loading due to the experimental simplicity. Although the data generated are useful from a fundamental point of view, the loads involved do not accurately reflect those typically experienced by engineering products in service. These loads are usually long term and static. For this reason, it is important to perform fracture tests under static fatigue conditions to establish a correlation between the findings of the short-term experiments and the fracture behaviour under static loads.

The same eleven HDPE copolymers were used as in Part I of this work. Static fatigue fracture testing was conducted in the double torsion test geometry using a multi-station loading rig. Double torsion was chosen as the test geometry because crack growth occurs at a constant rate for a considerable length of the specimen [2–4]. This permits the resistance to static fatigue to be conveniently expressed in terms of the rate of crack growth.

As in Part I of this work, the fracture behaviour has been related to the morphology and chain structure of the samples using a comprehensive statistical analysis. The findings will be discussed in terms of the Friedrich [5] model for fracture in HDPE. A comparison will also be made between the static fatigue data and the results from the tests conducted at a constant rate of deflection.

2. Experimental procedure

2.1. Material

Previous systematic studies of the relationship between static fatigue and the morphology and chain structure of HDPE have used either narrow molecular weight distribution fractions [6], or a series of whole polymers with widely varying characteristics [7–10]. This study is unique in that a series of whole polymers has been specially manufactured using commercial polymerization facilities. During the production of a single grade of resin the reactor conditions were

0022–2461

varied slightly, with the aim of producing samples of similar molecular weight distribution, but varying short branch content. A detailed description of the morphological and structural characterization of these resins was given in Part I [1]. For convenience, a summary of these results is reproduced in Table I.

2.2. Fracture analysis

2.2.1. The constant load rig

Static fatigue fracture measurements were made using the double torsion fracture geometry. In order to obtain multiple results in a reasonable time it was necessary to conduct testing using a number of independent test stations. A rig based on the double torsion geometry and consisting of twenty-two stations was designed by the authors and constructed in-house. A schematic representation of the loading system is shown in Fig. 1. The outer load points were 110 mm apart, whilst the separation of the inner load points was 35 mm. The steel spheres used as the loading points were 10 mm diameter. By use of a pre-calibrated force transducer, it was determined that the lever arm amplified the applied load by a factor of 19 at the specimen. This large magnification kept the weights that had to be handled to a manageable level. A counter balance was used to account for the mass of the lever arm.

2.2.2. Measurement of deflection

In static fatigue tests the load is held constant, and so to monitor the fracture process it is necessary to measure some other parameter as a function of time. Two suitable parameters are the crack opening displacement [9, 10] and the deflection of the loading point [7]. It is much easier to monitor deflection remotely than it is crack opening, and so deflection of the load point was chosen as the measurement parameter. This was done using a sliding linear resistor attached to the moving segment of the test rig (Fig. 1). Each resistor had a maximum movement of 25 mm, and could record the position to better than 0.03 mm. A dial micrometer was used to separately calibrate each resistor. The power supply was a stabilized 6 V source, trimmed to 5.0 V at each input by a second potentiometer. A JED Microprocessors data logger was used to record the variable output from the sliding resistor. The data logger was programmed to scan each test station at 15 s intervals, and store the data if the output had changed by 0.01 V or more. A typical load–deflection trace for HDPE in double torsion is shown in Fig. 2.

2.2.3. Test conditions

The specimens tested in static fatigue were of identical dimensions to those used in the constant displacement

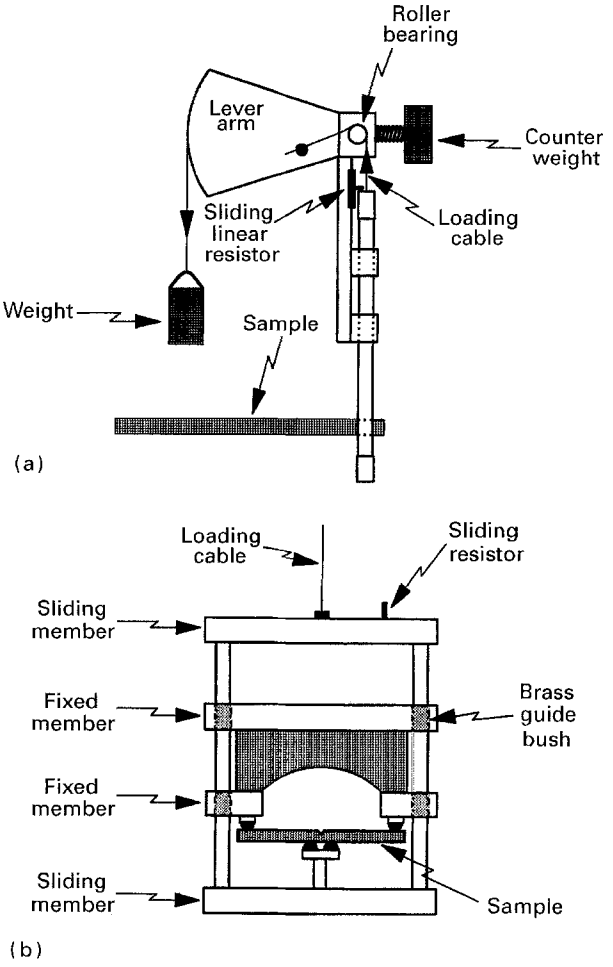

Figure 1 Schematic diagram of the static fatigue rig: (a) side view, (b) end view.

TABLE I Summary of experimental data characterizing the chain structure and morphology of the HDPE copolymers used in this work. Only variables for which significant variation occurred between the samples are listed

Sample	Comonomer type	$\bar{M}_n(10^{-4}$ Dalton)	$\bar{M}_w(10^{-5}$ Dalton)	Short branches/ 1000C	X_c (%)	L_c (nm)	L_a (nm)
A	1-butene	1.03 ± 0.03	1.30 ± 0.04	1.3 ± 0.1	73.93 ± 0.02	21.2 ± 1.0	11.2 ± 0.5
B	1-butene	1.00 ± 0.03	1.29 ± 0.04	1.9 ± 0.1	72.21 ± 0.06	19.9 ± 0.6	11.2 ± 0.3
C	1-butene	0.94 ± 0.03	1.24 ± 0.04	2.0 ± 0.1	72.46 ± 0.02	19.9 ± 0.2	11.2 ± 0.1
D	1-butene	0.94 ± 0.03	1.23 ± 0.04	1.1 ± 0.1	75.89 ± 0.04	22.3 ± 0.7	11.3 ± 0.3
E	1-butene	0.96 ± 0.03	1.33 ± 0.04	2.3 ± 0.1	72.09 ± 0.04	19.5 ± 0.1	11.1 ± 0.1
F	1-butene	1.07 ± 0.03	1.32 ± 0.04	3.2 ± 0.2	70.68 ± 0.06	18.1 ± 0.1	11.4 ± 0.1
G	1-butene	1.17 ± 0.04	1.39 ± 0.04	3.1 ± 0.2	71.32 ± 0.02	18.4 ± 0.2	11.6 ± 0.1
H	1-butene	1.08 ± 0.03	1.36 ± 0.04	2.7 ± 0.1	71.19 ± 0.08	17.9 ± 0.5	11.0 ± 0.3
I	1-butene	1.45 ± 0.04	1.53 ± 0.05	1.4 ± 0.1	72.21 ± 0.04	20.2 ± 0.3	12.2 ± 0.2
J	1-hexene	1.47 ± 0.04	1.01 ± 0.03	2.0 ± 0.1	71.19 ± 0.06	17.4 ± 0.7	11.8 ± 0.5
K	1-hexene	1.35 ± 0.04	0.90 ± 0.03	0.9 ± 0.1	76.83 ± 0.04	22.4 ± 0.3	10.3 ± 0.1

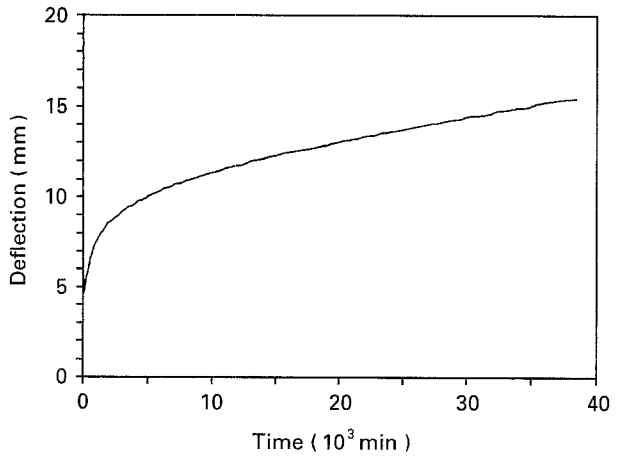

Figure 2 A typical deflection–time trace obtained in the static fatigue tests.

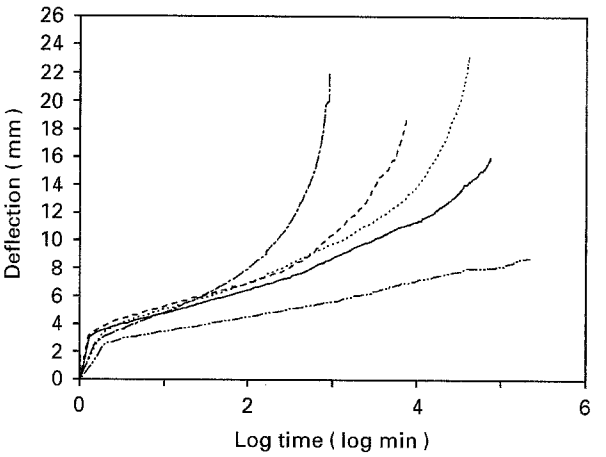

Figure 3 Comparison of static fatigue traces for selected samples at 25 °C under a load of 840 N. Sample: (– – –) K, (- - -) J, (- - -) D, (—) E, (– - - –) I.

rate tests [1]. Pre-cracking was performed as previously described for constant deflection rate tests [11]. For all resins except sample I, the initial sharp crack was grown at room temperature using a cross-head speed of 1 mm min^{-1}. The high toughness of sample I meant that it had to be pre-cracked at − 40°C.

Static fatigue testing was carried out over an 18 month period. Duplicate measurements were made at 25 ± 2.0° C using loads of 745 and 840 N at the sample. The load was applied through a pre-weighed container of lead shot. When initially applying a load, the container of lead shot was steadily released over a period of seconds until the sample had taken up the full load. Inspection of the load–deflection traces showed that the loading process occurred smoothly (Fig. 2).

An inter-sample comparison of the long term behaviour at a load of 840 N is shown in Fig. 3. For the sake of clarity only selected samples are shown. These samples represent the full range of fracture resistance observed.

2.2.4. Analysis of the deflection-time curve

In static fatigue the loads used typically generate stresses much lower than the initial yield stress. Given that the applied load is not too small, localized yielding will occur at the crack tip. This is often referred to as a damage zone. With time the damaged material will creep due to a fall in yield stress and modulus [12]. This creep causes the crack tip opening to increase to a critical size. A crack will then initiate and begin to extend. The period of time before a crack begins to propagate is called the incubation time, t_i. The value of t_i depends on the applied stress.

The total time to failure is the sum of the crack incubation and crack propagation times. In analysing static fatigue data it is necessary to break the total failure event into the initiation and propagation components. This is most conveniently done by expressing deflection versus time data on a log-linear graph [7, 12] (Fig. 4). This graph consists of three distinct stages. The primary stage is characterized by a rapid increase in deflection with time. This is associated with

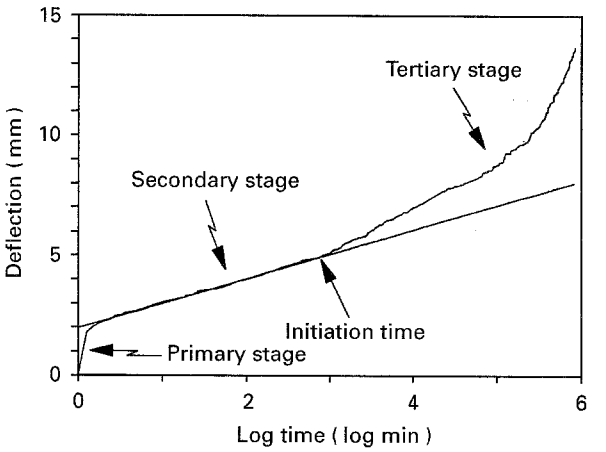

Figure 4 Illustration of the procedure used to determine the crack initiation time in static fatigue tests.

the take-up of the load, and has a duration of only a few minutes. In the secondary stage the deflection increases at a much slower rate than in the primary stage. During this period damage is accumulating at the crack tip. Crack initiation is marked by the onset of an acceleration in the rate of deflection. This is the tertiary stage of deformation, and this lasts until ultimate failure.

The incubation time, t_i, is the point of transition between the secondary and tertiary stages of deformation. To identify this point, a procedure similar to that described by Marshall [12] was used. Owing to the stable crack growth induced by the double torsion geometry, it was necessary to apply relatively high loads in order to obtain significant crack growth within the test period. Because of this, the measured incubation times were relatively short. For all samples (except sample I, for which no crack growth was observed) t_i was less than 500 min at loads of both 745 and 840 N. This is insignificant compared to the total time of the test. Furthermore, the inter-sample trend in t_i was different at the two test loads. This is a reflection of the low accuracy of the incubation data. When this is considered in conjunction with the low t_i values, it is clear that, in this work, incubation time is an unsatisfactory parameter against which to evaluate

the fracture behaviour of HDPE in static fatigue. As such, the long-term test results are limited to a study of crack propagation.

2.2.5. Fracture results

The parameter chosen to express the resistance to crack growth in static fatigue was the crack growth rate, $\dot{a}_{sf}$. Crack speeds were calculated using Equation 1 [13], where Δa is the distance of crack growth during time Δt, and P is the applied load. This procedure is satisfactory when using test geometries in which the crack grows at a constant rate, such as double torsion. For most specimens the test was interrupted prior to ultimate failure. The distance of crack growth, Δa, was evaluated by post-mortem analysis of the fracture surface. The difference between t_i and the time of unloading gave Δt. The largest error in $\dot{a}$ is that arising from poor estimates of the initiation time. Crack growth occurred over a period of thousands of minutes. On this scale the errors in t_i are relatively small. Thus, the crack-speed data are much more accurate than the initiation time results

$$\dot{a} = \left(\frac{\Delta a}{\Delta t}\right)_P \quad (1)$$

Average crack speeds for the tests conducted at 25° C using loads of 745 and 840 N are presented in Table II.

TABLE II Summary of experimental data characterizing the resistance to crack propagation under static loads. Measurements were made at 25 °C using the indicated loads

Sample	$\dot{a}$ (mm h^{-1})	
	745 N	840 N
A	0.053	0.11
B	0.042	0.079
C	0.035	0.070
D	0.037	0.087
E	0.006	0.017
F	0.005	0.018
G	0.010	0.026
H	0.014	0.039
I	–	–
J	0.14	0.47
K	2.80	10.8

Because measurements were only made in duplicate it is not possible to estimate the errors in the data. However, there was substantial scatter in the results. Despite this, the inter-sample trend was similar at each load. This gives increased confidence in the accuracy of the crack-speed results. Owing to the similarity in the trend of both sets of data, only the results at a load of 840 N were used to interpret resistance to slow crack growth in terms of morphology and chain structure.

3. Statistical analysis

Statistical analysis of the fracture data in Part I of this work was performed for two sets of samples, these being samples A–H and samples A–I. The set excluding sample I was chosen in order to minimize molecular weight variation, and so allow the influence of other morphology and chain structure variables to be examined. However, in the static fatigue experiments, no crack growth was observed for sample I. Because a value of $\dot{a}_{sf}$ is not available for sample I, a statistical analysis on the $\dot{a}_{sf}$ data of samples A–I could not be performed. Samples J and K were not included in the statistical analysis because they were manufactured using a different comonomer, and with a different catalyst system. However, a comparative analysis of the role of comonomer type will be presented.

The statistical methodology used for the static fatigue data was exactly the same as that described in Part I of this work [1]. A backward stepwise regression was used to screen those variables which significantly influenced the fracture parameter, $\dot{a}_{sf}$. To improve the accuracy of the regression coefficients the stepwise regression was followed by a ridge regression. The final regression model fitted to the fracture data was of the form shown in Equation 2. Results of the stepwise and ridge regressions are summarized in Tables III and IV, respectively. A null entry in these tables indicates that the variable in question was removed from the model during the stepwise screening procedure. These variables do not significantly influence the corresponding fracture parameter.

$$y = \beta_0 + \beta_1 x_1 + \beta_2 x_2 + \cdots + \beta_n x_n \quad (2)$$

TABLE III Stepwise regression coefficients for the relationship between resistance to crack growth and the morphology and chain structure of samples A–H

Fracture parameter	Stepwise regression coefficients, β						
	β_0	$\bar{M}_n(10^{-4})$	$\bar{M}_w(\times 10^{-5})$	SCB($\times 10^2$)	$L_c(\times 10^{-2})$	L_a	R^2
$\dot{a}_{sf}$	0.88	0.41	− 0.49	− 8.5	− 0.21	–	0.98

TABLE IV Coefficients of the ridge regression performed on the set of screened variables listed in Table III

Fracture parameter	Ridge regression coefficients, β^*						
	β_0^*	$\bar{M}_n(\times 10^{-5})$	$\bar{M}_w(\times 10^{-5})$	SCB ($\times 10^{-1}$)	$L_c(\times 10^{-3})$	$L_a(\times 10^{-3})$	R^2
$\dot{a}_{sf}$	7.0E-2	0.84	− 0.12	− 0.22	0.55	–	0.81

4. Discussion

4.1. Fracture model

The best way to interpret the results of the statistical analysis is to review them in terms of a descriptive model of the fracture process. In the earlier part of this work the model proposed by Friedrich [5] was used. This model has been verified by direct microscopic observations [14–16]. Because a detailed description of this model has previously been presented [1], a brief summary is all that will be given here.

The precursor to failure in polyethylene is crazing. For a crack to grow the fibrils joining the surfaces of a craze must rupture. Fibrils rupture as the link molecules that hold them together become disentangled and slide past each other. During the time it takes for the link molecules completely to disentangle, the fibrils are drawn out in length. An increase in the density of link molecules results in the applied stress being transferred more effectively throughout the fibril, the average stress per tie chain being lower, and each link molecule becoming more extensively entwined with other structural elements. These features make chain disentanglement more difficult and so prolong the process of fibril extension prior to rupture. Because the fibrils must be drawn to greater lengths, fewer fibrils will be broken per unit time. This is tantamount to a reduced crack speed. Thus, an increased difficulty of chain slip results in an enhanced resistance to crack propagation due to a lower rate of fibril failure.

The Friedrich model is based on deformations occurring at moderate rates of loading. The relative importance of fibril extension as opposed to chain disentanglement is expected to change with variations in loading rate. Lustiger and Markham [17] have extended the model to account for the effect of strain rate. In static fatigue tests a specimen fails under a moderate load over a long period of time. Such time scales permit stressed link molecules to relax by reptation. Some link chains will pull out of the crystals without causing large-scale fibrillation. Eventually there will be too few links remaining to support the load, and the material will fail in a macro-brittle manner. Under these conditions the extent of crystal unfolding is expected to be less extensive than in constant deflection rate tests. However, some crystal unfolding will occur, and so energy absorption through this mechanism will still be an important component of the fracture process in static fatigue.

4.2. Interpretation of statistical analysis

The results of the statistical analysis on $\dot{a}_{sf}$ are not as straight forward to interpret as for the constant deflection rate data [1]. This may be due to the presence of more scatter in the static fatigue results. Lower accuracy of the $\dot{a}_{sf}$ data makes it harder for the statistical model to determine which of the variables are important in influencing crack speed.

4.2.1. Samples A–H

A positive correlation between the resistance to slow crack growth and weight average molecular weight was observed for samples A–H. Such a relationship is expected. Even though chain pull-out is easier in long-term tests, it will take longer for the sample to fail if a larger number of link molecules have to untangle. The reasons for this were outlined above. It is well established that link density increases with molecular weight [17, 18].

The statistical analysis predicted a decrease in the resistance to crack growth with an increase in the number average molecular weight of samples A–H. This result is not understood. There is no reasonable explanation as to why the crack speed should increase as the molecules become longer. This finding is also contrary to the trend predicted by a straight comparison of $\dot{a}_{sf}$ and $\bar{M}_n$ (Fig. 5). It is interesting to note that if the amount of bias in the ridge regression is allowed to become sufficiently high, then the coefficient of $\bar{M}_n$ does become negative (Fig. 6). However, the goodness of fit of a model with such a large amount of bias is poor. Owing to uncertainty over the direction in which $\bar{M}_n$ influences $\dot{a}_{sf}$, it is not possible to make a meaningful interpretation as to why $\bar{M}_n$ was included in the statistical model.

For samples A–H, the resistance to crack growth under small, static loads was observed to increase with the degree of short chain branching. This is understood in terms of short branches acting as protrusions along the polymer chain. Being short, these protrusions are fairly inflexible, and so make it more difficult for the link molecules to be pulled through crystalline blocks. This prolongs the time it takes for the chains to reptate free of entanglements. Consequently, the rate of slow crack growth is reduced.

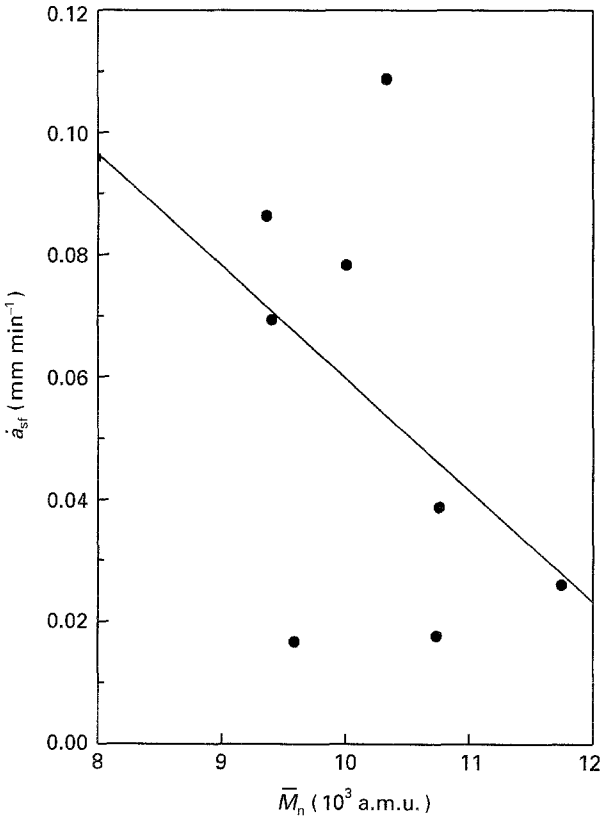

Figure 5 Crack speed in static fatigue versus number average molecular weight, samples A–H. Correlation coefficient, $r = -0.42$.

The resistance to crack growth in static fatigue was found to be significantly enhanced by a reduction in crystal thickness. This is opposite to the relationship that would be predicted from the model proposed by Lustiger and Markham [17]. In this model it is assumed that crack speed decreases with increasing crystal thickness, because a greater length of molecule is encapsulated by thick crystals. This will make chain pull-out more difficult. For this assumption to hold true, it is necessary that the increased difficulty of chain slip does not cause the lamellae to unfold. This is likely to be true if the applied load is low. However, at higher loads the stress acting on the crystal surfaces is larger, and the time available for reptation is reduced. The combined action of these factors means that lamellar unfolding becomes more extensive as the static load is increased.

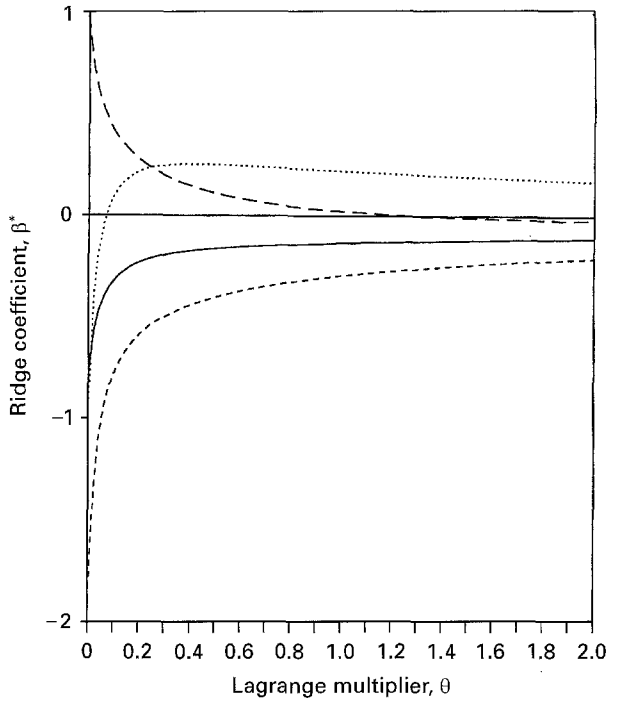

Figure 6 Ridge trace for static fatigue crack speed data of samples A–H, extended to large values of θ. The magnitude of θ indicates the amount of bias in the model. Coefficients for: (——) $\overline{M}_w$, (– – –) $\overline{M}_n$, (- - -), SCB, (···) L_c.

The static fatigue data in the present work were generated using relatively high loads. This results in fibril extension playing a more dominant role than envisaged by Lustiger and Markham. The molecular mechanisms responsible for the observed improvement in resistance to slow crack growth with a reduction in crystal thickness are similar to those outlined for the constant deflection rate data [1]. Briefly, these are that thinner crystals yield more easily, resulting in fibrillation over a greater volume, and more extensive elongation of the fibrils. The combined effect of a larger number of longer fibrils is to retard the rate of crack opening, and so give increased resistance to crack propagation.

4.2.2. Samples A–I

A crack did not initiate in sample I during 5 months of testing at 840 N. Consequently, a statistical analysis of the $\dot{a}_{sf}$ data of samples A–I could not be performed. However, the difficulty of growing a crack in sample I re-emphasizes the extremely important role of molecular weight in enhancing resistance to static fatigue. Sample F has the highest resistance to static fatigue among samples A–H, and one of the highest average molecular weights. Over the same time period in which no crack extension was observed in sample I, a crack in sample F initiated and grew to a length of $\sim$35 mm. The difference in molecular weight of these two resins is 15% for $\bar{M}_n$ and 35% for $\bar{M}_w$. Such a high sensitivity of static fatigue resistance to molecular weight can be attributed to the increased importance of link molecule disentanglement in long-term tests.

4.3. Influence of short branch length

As in Part I of this work, the effect of comonomer type was analysed descriptively using selected sample pairs. Samples D and H, which are ethylene 1-butene copolymers, were compared with samples J and K, both of which contain 1-hexene as a comonomer. The various properties of these resins are listed in Table V.

TABLE V Comparison of properties between butyl branched resins and ethyl branched resins

		Ethyl branched resins			Butyl branched resins		
		Sample D	Sample H	% change D–H	Sample K	Sample J	% change K–J
Chain structure	$\bar{M}_n$ (a.m.u.).	9 350	10 760	15	13 500	14 650	9
	$\bar{M}_w$ (a.m.u.).	123 100	135 900	10	89 950	101 200	13
	SCB (/1000C)	1.1	2.7	145	0.9	2.0	122
Morphology	L_c (nm)	19.5	17.9	−8	22.4	17.4	−22
	L_a (nm)	11.1	11.0	−1	11.8	10.3	−15
Fracture behaviour	$\dot{a}_{sf}$ (mm h^{-1})	0.087	0.039	−55	10.8	0.47	−96

A strong dependence of crystal thickness on comonomer content is established in the literature [19–22]. The increase in short branch concentration between samples K and J is approximately the same as between samples D and H. However, the reduction in crystal thickness between the two 1-hexene resins is almost three times that for the 1-butene resins. This suggests that longer short branches are more effective at inhibiting the crystal thickness.

The increase in resistance to crack propagation, ($\dot{a}_{sf}$), was twice as large for the 1-hexene pair than for the 1-butene pair. The statistical analysis of samples A–H showed that $\dot{a}_{sf}$ was significantly influenced by crystal thickness. Because 1-hexene comonomer reduces crystal thickness to a greater extent than does 1-butene, it appears that incorporating comonomers with longer side-groups into HDPE resins will further reduce the crystal thickness, and so will increase the resistance to crack growth under static loading conditions. This is identical to the result obtained for the constant deflection rate tests.

5. Conclusion

The resistance to crack propagation under static loads, ($\dot{a}_{sf}$), was measured using the double torsion fracture geometry. The resistance to crack growth was found to increase with molecular weight, decrease with crystal thickness, and increase with short branch concentration. These findings are similar to earlier conclusions drawn from work conducted at a constant rate of deflection. This is a valuable correlation, because the constant deflection rate tests are conducted over a much shorter time frame. As a result, it is possible that an early indication of the likely long-term performance of HDPE products under static loads can be obtained from rapid comparative tests conducted on a tensile testing machine.

Some evidence was presented to indicate that molecular weight influences fracture behaviour to a greater extent in long-term tests than in constant deflection rate tests. This can be attributed to link molecules having more time to reptate free of entanglements in static fatigue tests. As a result, chain slip plays a more dominant role in the total fracture process. A higher molecular weight results in a greater number of link molecules, and so the rate of chain slip, and hence crack propagation, is slower. This result indicates that molecular weight is a most critical parameter when considering the long-term performance of HDPE materials.

Changes in molecular weight that are commercially possible are restricted by processing requirements. When the allowable variation in molecular weight is small, the resistance to static fatigue can still be enhanced by raising the short branch content. Furthermore, there is some evidence to suggest that the use of higher 1-olefin comonomers provides a more effective means of inhibiting the static fatigue process. These results are again consistent with the findings from tests conducted at a constant rate of deflection, and are of significant commercial interest.

References

1. B. J. EGAN and O. DELTAYCKI, *J. Mater. Sci.* (1994) submitted.
2. R. FRASSINE, T. RICCÒ, M. RINK and A. PAVAN, *ibid.* **23** (1988) 4027.
3. J. A. KIES and B. J. CLARK, in "Proceedings of the 2nd International Conference on Fracture", Brighton, April 1969, edited by P. L. Pratt (Chapman and Hall, London, 1969) p. 483.
4. J.-C. POLLET and S. J. BURNS, *J. Am. Ceram. Soc.* **62** (1979) 426.
5. K. FRIEDRICH, *Adv. Polym. Sci.* **52–53** (1983) 225.
6. V.V. MATVEYEV, A. YA. GOL'DMAN, V. P. BUDTOV, YE. L. PONOMAREVA and A. M. LOBANOV, *Polym. Sci. USSR* **21** (1979) 413.
7. D. C. BASSET, A.M. HODGE and R. H. OLLEY, *Farad. Soc. Disc.* **68–69** (1979–80) 218.
8. J. M. CRISSMAN and L. J. ZAPAS, in "Durability of Macromolecular Materials", edited by R. K. Eby (ACS Symposium Series 95, Washington, DC, 1979) p. 289.
9. X. LU, X. WANG and N. BROWN, *J. Mater. Sci.* **23** (1988) 643.
10. Y. L. HUANG and N. BROWN *ibid.* **23** (1988) 3648.
11. B. J. EGAN and O. DELTAYCKI, *ibid.* **29** (1994) 6026.
12. G. P. MARSHALL, *Plast. Rubber Proc. Appl.* **2** (1982) 169.
13. P. W. R. BEAUMONT and R. J. YOUNG, *J. Mater. Sci.* **10** (1975) 1334.
14. W. W. ADAMS, D. YANG and E. L. THOMAS, *ibid.* **21** (1986) 2239.
15. J. M. BRADY and E. L. THOMAS, *ibid.* **24** (1989) 3311.
16. *Idem, ibid.* **24** (1989) 3319.
17. A. LUSTIGER and R. L. MARKHAM, *Polymer* **24** (1983) 1647.
18. L. MANDELKERN and A. J. PEACOCK, in "Proceedings of an International Course and Conference on the Interfaces between Mathematics, Chemistry and Computer Science", Dubrovnik, Yugoslavia, 1987, edited by R. C. Lacher (Elsevier Applied Science, New York, 1988) p. 201.
19. R. ALAMO and L. MANDELKERN, *Macromolecules* **22** (1989) 1273.
20. F. ANIA, H. G. KILIAN and F. J. BALTÁ CALLEJA, *J. Mater. Sci. Lett.* **5** (1986) 1183.
21. F. J. BALTÁ CALLEJA, J. C. GONZÁLEZ ORTEGA and J. MARTINEZ DE SALAZAR, *Polymer* **19** (1978) 1094.
22. G. BODOR, H. J. DALCOLMO and O. SCHRÖTER, *Coll. Polym. Sci.* **267** (1989) 480.

Received 30 June 1994
and accepted 20 January 1995